Journal of Materials Science and Chemical Engineering, 2023, 11, 22-33
https://www.scirp.org/journal/msce
ISSN Online: 2327-6053
ISSN Print: 2327-6045

The Advent of Wide Bandgap Green-Synthesized Copper Zinc Tin Sulfide Nanoparticles for Applications in Optical and Electronic Devices

Opeyemi S. Akanbi[1], Haruna A. Usman[2], Gbemi F. Abass[3], Kehinde E. Oni[4], Akinsanmi S. Ige[1], Bola P. Odunaro[5], Idowu J. Ojo[6], Julius A. Oladejo[7], Halimat O. Ajani[1], Adnan Musa[8], Joshua Ajao[6]

[1]Department of Pure and Applied Physics, Ladoke Akintola University of Technology, Ogbomosho, Nigeria
[2]Department of Mechanical Engineering, Jigawa State Polytechnic, Dutse, Nigeria
[3]Department of Materials Science and Engineering, Hohai University, Nanjing, China
[4]Department of Mechanical Engineering, Ekiti State University, Ado Ekiti, Nigeria
[5]Department of Materials Science and Engineering, University of Colorado Boulder, Boulder, USA
[6]Department of Chemical Engineering, Ladoke Akintola University of Technology, Ogbomoso, Nigeria
[7]Department of Mechanical Engineering, Federal University of Technology, Akure, Nigeria
[8]Department of Biotechnology and Genetics, Russian State Agrarian University, Moscow, Russia
Email: akanbiopeyemisamson@gmail.com, igeakinsanmi@gmail.com, ajaniwumih@gmail.com, haruna.abbausman19@jigpoly.edu.ng, abass.gbemi@gmail.com, onikehinde21@gmail.com, odunarobolapius@gmail.com, ajaojoshua123@gmail.com, ijojo30@student.lautech.edu.ng, aanuoluwajulius@gmail.com, mrvixible@gmail.com

How to cite this paper: Akanbi, O.S., Usman, H.A., Abass, G.F., Oni, K.E., Ige, A.S., Odunaro, B.P., Ojo, I.J., Oladejo, J.A., Ajani, H.O., Musa, A. and Ajao, J. (2023) The Advent of Wide Bandgap Green-Synthesized Copper Zinc Tin Sulfide Nanoparticles for Applications in Optical and Electronic Devices. *Journal of Materials Science and Chemical Engineering*, **11**, 22-33.
https://doi.org/10.4236/msce.2023.113002

Received: February 8, 2023
Accepted: March 26, 2023
Published: March 29, 2023

Abstract

Power-electronic devices are widely used in various applications, such as voltage and frequency control for transmitting and converting electric power. As these devices are becoming increasingly important, there is a need to reduce their losses and improve their performance to reduce electric power consumption. Current power semiconductor devices, such as inverters, are made of silicon (Si), but the performance of these Si power devices is reaching its limit due to physical properties and energy bandgap. To address this issue, recent developments in wide bandgap (WBG) semiconductor materials, such as silicon carbide (SiC) and gallium nitride (GaN), offer the potential for a new generation of power semiconductor devices that can perform significantly better than silicon-based devices. In this research, a green synthesized copper-zinc-tin-sulfide (CZTS) nanoparticle is proposed as a new WBG semiconductor material that could be used for optical and electronic devices. Its synthesis, consisting of the production methods and materials used, is discussed. The characterization is also discussed, and further research is recommended in the later sections to enable the continual advancement of this technology.

Keywords

Wide Bandgap Semiconductor, Semiconductor, Electronic Device, Power Device, Optical Device, CZTS

1. Introduction

A semiconductor with a "wide bandgap" has considerable energy (forbidden bandgap), as the name suggests, which is closely related to optical devices' absorption and emission wavelengths. The emission and absorption wavelengths of typical wide bandgap semiconductors extend into the shorter wavelengths of violet and ultraviolet light and the green and blue portions of the visible spectrum. Wide bandgap semiconductors, for instance, are used in well-known devices like "blue light emitting diodes". Wide-bandgap semiconductors are, therefore, often thought to have fundamental optical absorption edges with wavelengths shorter than red. Light-emitting diodes, laser diodes, photodiodes, photoconductive sensors, electro-modulation devices, and optical-optical modulation devices are a few examples of optical devices [1]. Compared to traditional light sources, semiconductor light-emitting devices are incredibly tiny, light in weight, highly efficient, and have far longer lives. Wide bandgap semiconductors, in particular, have grown in significance in the electronics sector as optical components for full-color displays, white light lighting, UV/deep UV light sources, and blue-violet laser diodes for high-density DVDs. But despite the widespread interest in using wide-bandgap semiconductors for blue LEDs, it took a while before technological advances allowed the creation of PN junctions in GaN. Wide bandgap (WBG) semiconductor device integration as a replacement for silicon technology is a developing market that can offer increases in efficiency and power density, which significantly affect energy and cost reductions [2]. Essential benefits of WBG include higher switching frequencies, less power loss, and increased power density. Thus, more commitment from scientists toward research must bring about more materials (wide bandgap semiconductors) that could be used to advance other areas of the industry. The need for cost-effective and environmentally friendly alternatives to traditional semiconductor materials has driven the development of green synthesized copper zinc tin sulfide nanoparticles. This quaternary compound can be synthesized using a simple, green chemical process involving the mixing of copper, zinc, and tin sulfate solutions, making it highly scalable and easily adaptable for industrial production. Its wide-bandgap properties make it a promising candidate for use in optical and materials technologies. To assess its potential, optical analysis was conducted on samples in various proportions, as well as when adding polar and non-polar solvents. Results showed that each sample had a different bandgap.

Introduction to Wide Bandgap (WBG) Device Applications

In 2014, data centers in the United States used around two percent of the nation's electricity demand [2]. The majority of modern data centers feature a line frequency transformer, low voltage power distribution network, centralized backup unit, and ineffective voltage regulators. To increase the energy efficiency of data centers, tactics such as the incorporation of reduced-loss power converters and a complete overhaul of the power delivery network are employed. To further restructure the power distribution network, higher voltages must be converted at the rack level, requiring careful consideration of thermal management and space constraints. It is also important to note that increased temperature tolerance can reduce cooling loads and boost the grid-to-chip efficiency of data centers, making high-power density converters based on Wide Band Gap (WBG) devices a key enabler for more efficient systems.

The aerospace sector stands to benefit from WBG-based technology in the form of longer, thinner, and lighter wings which are reported to consume less fuel and emit fewer greenhouse gases than existing commercial aircraft. This would result in significant annual energy savings, but a radical wing design using electromechanical actuators is needed [3] [4]. These actuators must be compact, lightweight, and able to operate effectively across a range of temperatures. Moreover, WBG-based converters can provide an energy-efficient way of electrifying the wings to lighten them and improve performance.

Power conditioning is essential for regulating the flow of electricity in grid-connected systems such as solar and wind power, high voltage direct current (HVDC), and flexible alternating current transmission systems (FACTS). This ensures that the right currents and voltages are supplied to the load. Traditional silicon power electronics can be a source of failure as they cause a 4% loss of electricity in such applications. By operating at higher switching frequencies, novel wide-bandgap (WBG) circuits reduce system costs and improve system efficiency by allowing PV arrays to function at higher voltages. Ultimately, this could mean replacing conventional combiner boxes in DC systems with fewer voltage conversions or transformers.

2. Experimental

2.1. Materials and Methods

The green synthesized copper-zinc-tin-sulfide nanoparticles were achieved by mixing a measurable portion of the plant extract with a solution that consists of a mixture of CZTS precursors. The method used is the chemical precipitation method, and the resulting precipitate is then heated at an elevated temperature to form green synthesized CZTS nanoparticles. The plant extraction consisting of *Vernonia amygdalina* and *Ocimum gratissimum* leaves is further discussed in Subsection 2.2.

2.1.1. Equipment

The equipment used is a magnetic stirrer (used for stirring throughout the expe-

riment), magnetic bar, water dispenser, mortar, pestle, measuring cylinder, beaker, sensitive weighing balance, hot plate, petri dish, spatula, and funnel.

2.1.2. Chemicals and Solvent

Thiourea and Sodium Sulphate Anhydrous were used as a source of sulfur precursor. Ammonia Solution was used to control the pH. Distilled water was used as a solvent for the synthesis. Zinc Nitrate ($Zn(NO_3)_2{\cdot}6H_2O$) is a zinc precursor source. Triethanolamine was used as a complexing agent. Tin Sulphate is used as a source of Tin. Copper (II) sulfate pentahydrate ($CuSO_4{\cdot}5H_2O$) is a copper precursor source. Acetone was employed as a non-polar solvent to dissolve the powdered leaves of *Vernonia amygdalina* and *Ocimum gratissimum*, which were initially dried and ground at room temperature. Meanwhile, methanol was employed as a polar solvent to dissolve the same dried, ground leaves at the same temperature.

2.2. Sample Preparation

2.2.1. Preparation of Leaf Extract Sample

The *Vernonia amygdalina* and *Ocimum gratissimum* leaves were separately washed using distilled water, dried at room temperature, and powdered using the mortar and pestle. 20 g each of the powdered leaves was dissolved in a container containing 20 cl acetone and 20 cl methanol. That is:

Solution A: 20 g of *Vernonia amygdalina* + 20 cl acetone

Solution B: 20 g of *Vernonia amygdalina* + 20 cl methanol

Solution C: 20 g of *Ocimum gratissimum* + 20 cl acetone

Solution D: 20 g of *Ocimum gratissimum* + 20 cl methanol

2.2.2. Preparation of Chemical Sample

The precursors, Thiourea Sodium Sulphate Anhydrous, Ammonia Solution, Zinc Nitrate ($Zn(NO_3)_2{\cdot}6H_2O$), Triethanolamine, Tin Sulphate, Copper (II) sulfate pentahydrate ($CuSO_4{\cdot}5H_2O$) in 0.01 mol of each were dissolved in 10 ml of distilled water. The proportion of the precursor was obtained through the following mathematical equation;

$$C_1 = \frac{C_2 \times V_2}{V_1}$$

where C_1 is the unknown concentration of the precursors in grams, C_2 is the known concentration of the precursors, gotten by: C_2 (concentration in gram) = molarity (concentration in mole) × molar mass (concentration in g/mol). V_1 is the standard volume of 1000 ml, and V_2 is the known volume where the precursors are dissolved; it is the volume of the distilled water, thus V_2 = 10 ml.

Proportions:

10 ml of Ammonia Solution and Triethanolamine;

For Sodium Sulphate Anhydrous (Na_2SO_4), molar mass = 142.04 g/mol

C_1 = (0.01 mol × 142.04 g/mol × 10 ml)/(1000 ml) = 0.014204 g

For Zinc Nitrate ($Zn(NO_3)_2{\cdot}6H_2O$), molar mass = 297.48 g/mol

C_1 = (0.01 mol × 297.48 g/mol × 10 ml)/(1000 ml) = 0.029748 g

For Thiourea, molar mass = 76.12 g/mol

C_1 = (0.01 mol × 76.12 g/mol × 10 ml)/(1000 ml) = 0.007612 g

For Tin Sulphate, molar mass = 100 g/mol

C_1 = (0.01 mol × 100 g/mol × 10 ml)/(1000 ml) = 0.01 g

For Copper (II) sulphate pentahydrate ($CuSO_4 \cdot 5H_2O$), molar mass = 249.68 g/mol

C_1 = (0.01 mol × 249.68 g/mol × 10 ml)/(1000 ml) = 0.024968 g

The solution consisting of the precursors in the above proportion, dissolved in 10 ml of distilled water, and stirred for proper dissolution is referred to as solution E.

Sample F: it contains solution A plus 30 ml of solution E

Sample G: it contains solution B plus 30 ml of solution E

Sample H: it contains solution C plus 30 ml of solution E

Sample I: it contains solution D plus 30 ml of solution E

The solutions F, G, H, and I was stirred for 90 minutes at 900C on the magnetic stirrer. Then, it was filtered, and the residue was allowed to dry. Thus, the dry residue of solutions F, G, H, and I is the synthesized CZTS.

3. Results and Discussion

The evolution of the optical properties of the prepared CZTS nanoparticle was determined after obtaining the transmittance spectrum.

3.1. UV-Vis Spectrophotometer

In UV-Vis spectroscopy, the data obtained have a wavelength (nanometer) and transmittance (in percentage) [5]. The absorbance was calculated using Beer's law from the percentage transmittance data. The formula is given by $A = 2 - \log_{10}(\%T)$, and **Figures 1-4** shows the UV-Vis absorbance spectrum.

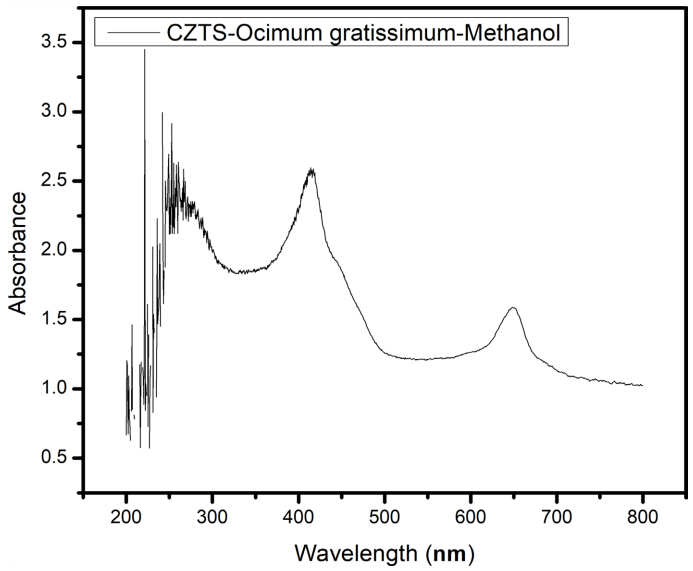

Figure 1. UV-Vis spectrum of Sample I.

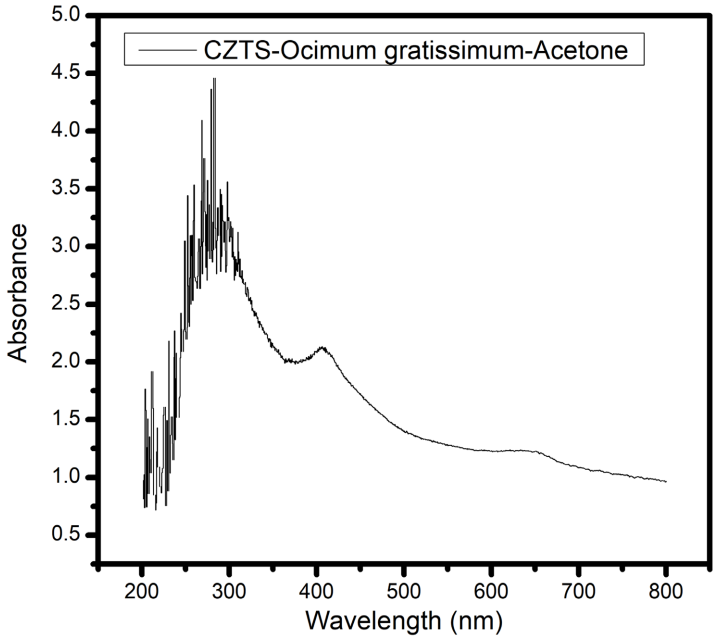

Figure 2. UV-Vis spectrum of Sample H.

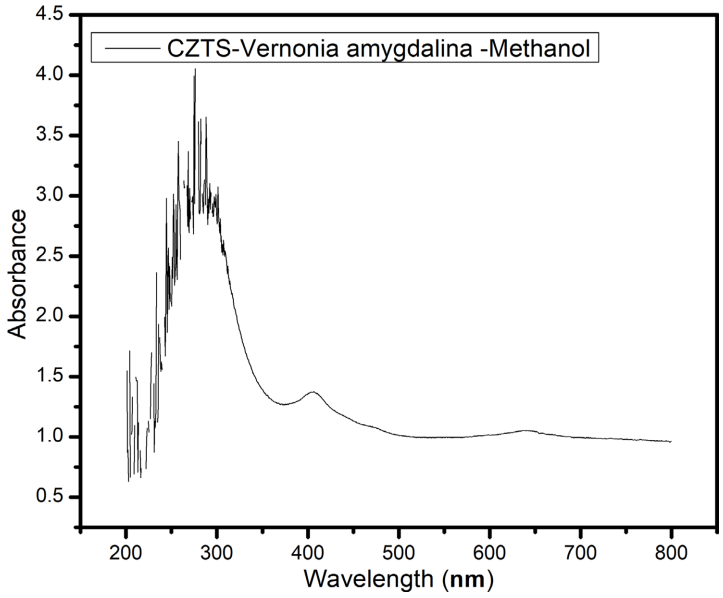

Figure 3. UV-Vis spectrum of Sample G.

The optical bandgap energy was calculated from the absorption data using the Tauc plot method. The equation, $(\alpha h\upsilon)^n = K(h\nu - E_g)$ is known as Tauc and Davis-Mott relation. This relation is used to probe the optical bandgap energy of nanoparticles from UV-Vis absorption spectroscopy. In this equation, "α" is the absorption coefficient, "$h\upsilon$" is the incident photon energy, "K" is the energy-independent constant and Egis the optical bandgap energy of the nanoparticle. In this equation, the exponential "n" represents the nature of the transition. For direct bandgap material, $n = 2$ while for indirect $n = 1/2$. In the Tauc plot method, we plot energy on the x-axis while $(\alpha h\upsilon)^n$ on the y-axis. Then a tangent

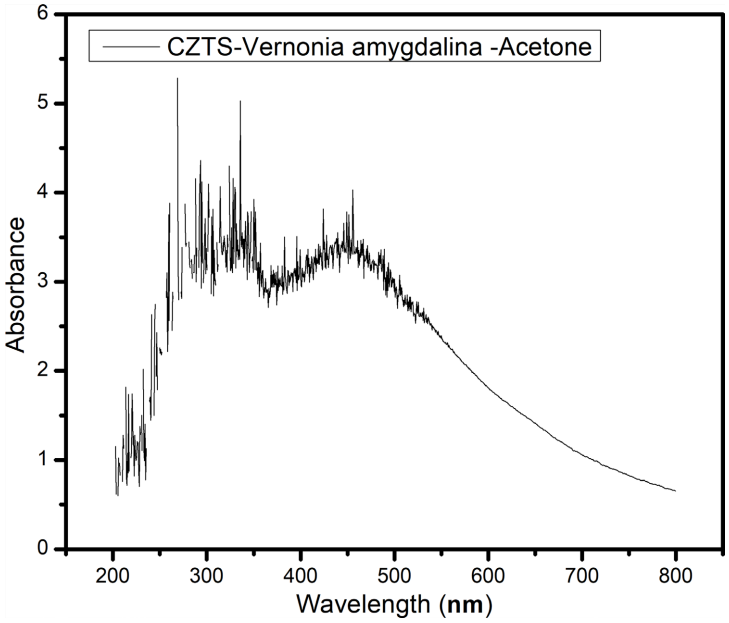

Figure 4. UV-Vis spectrum of Sample F.

line on the curve where $\alpha = 0$ is drawn to touch the x-axis to give the value of the optical bandgap energy of the material.

Absorption coefficient (α) was calculated from the absorption data using Beer-Lambert's law ($I/I_0 = \mathrm{e}^{-\alpha L}$) here I is the intensity of the transmitted light and I_0 is the intensity of the incident light, and L is the path length of light through which absorbance takes place. From Beer Lambert's law, $\log(I/I_0) = \alpha L \log(\mathrm{e})$. But Absorbance $A = \log(I/I_0)$ and $1/\log(\mathrm{e}) = 2.303$. So $\alpha = 2.303A/L$. L can be calculated from the standard quarks cuvette length that is used in the spectrophotometer. In this case, L = 10 mm or 1 cm, which is the path length of the cuvette. Absorbance, $\alpha = 2.303A\ \mathrm{cm}^{-1}$ then $(\alpha h\upsilon)^n = (2.303 \times A \times h\nu)^n$, with the unit ($\mathrm{eVcm}^{-1}$). The linear part of the curve is extrapolated, and the intercept is the bandgap of the material shown in **Figures 5-8**.

In order to accurately calculate the bandgap, **Figures 5-8** show that the mechanism used to select the appropriate curve region for the tangent is to determine which line of intercept provides the most accurate approximation, as outlined by Makuła, Pacia, & Macyk (2018) [5].

3.2. Fourier Transform Infrared (FTIR) of Synthesized CZTS

CZTS nanoparticles were characterized with Fourier Transform Infrared (FTIR) spectrum, which gives pattern images in **Figures 9-12**. The chemical compositions of the synthesized CZTS nanoparticles were studied; the structural design of the CZTS nanoparticles obtained was analyzed by using Fourier Transform Infrared (FTIR) spectrometer.

In **Figure 9**, the bond at 3278.96 has O-H (Alcohol) stretch characteristics, and the peak at 1605.96 represents a (C=C) functional group. In **Figure 10**, the peak at 3354.54 has characteristics of an O-H (Alcohol) stretch, while the bond

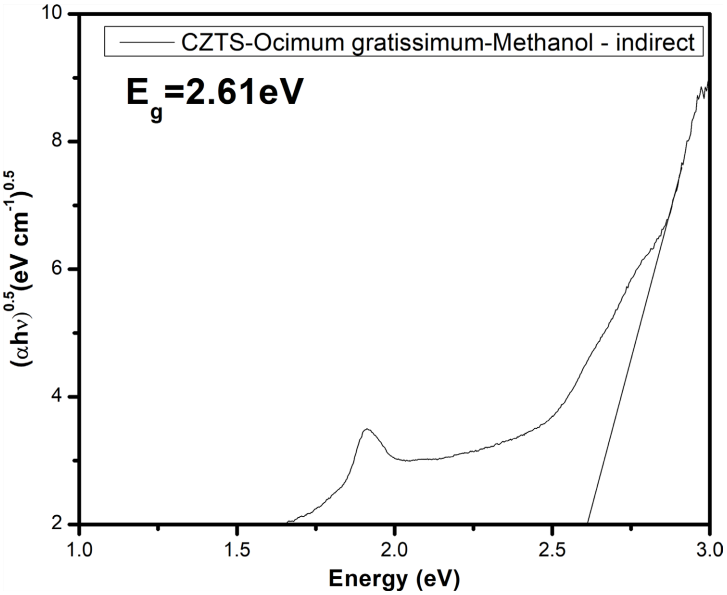

Figure 5. Tauc plot showing the bandgap of Sample I.

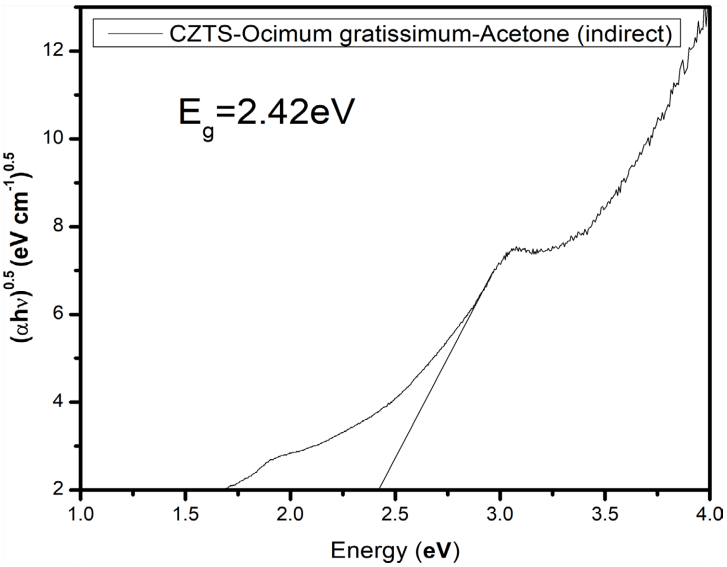

Figure 6. Tauc plot showing the bandgap of H.

at 2931.66 is characteristic of a C-H stretch. In **Figure 11**, the peak at 3354.45 is characteristic of an O-H (Alcohol) stretch; the peak at 2931.77 is characteristic of a C-H bond stretch, and the peak at 1654.22 represents the (C=C) bond.

In **Figure 12**, the peak at 3354.18 is characteristic of an O-H (Alcohol) stretch; the peak at 2931.77 is characteristic of a C-H stretch, and the peak at 1611.19 represents the (C=C) bond.

The FTIR analysis of bond attribution was outlined by Khan *et al.* (2018) [6].

4. Conclusion and Recommendation

It appears that the various CZTS synthesized through green methods have a wide bandgap, and their optical properties, as demonstrated by the varying

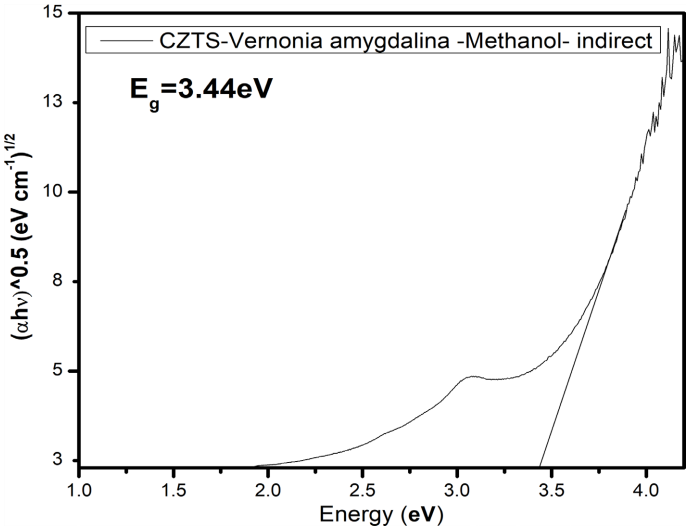

Figure 7. Tauc plot showing the bandgap of Sample G.

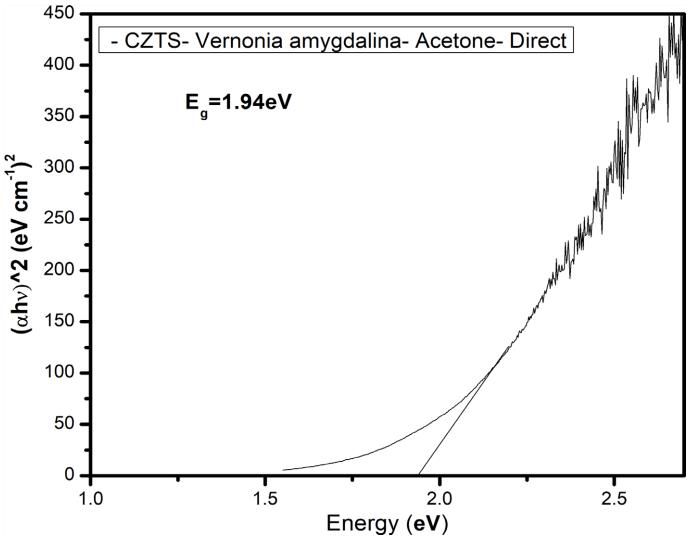

Figure 8. Tauc plot showing the bandgap of Sample F.

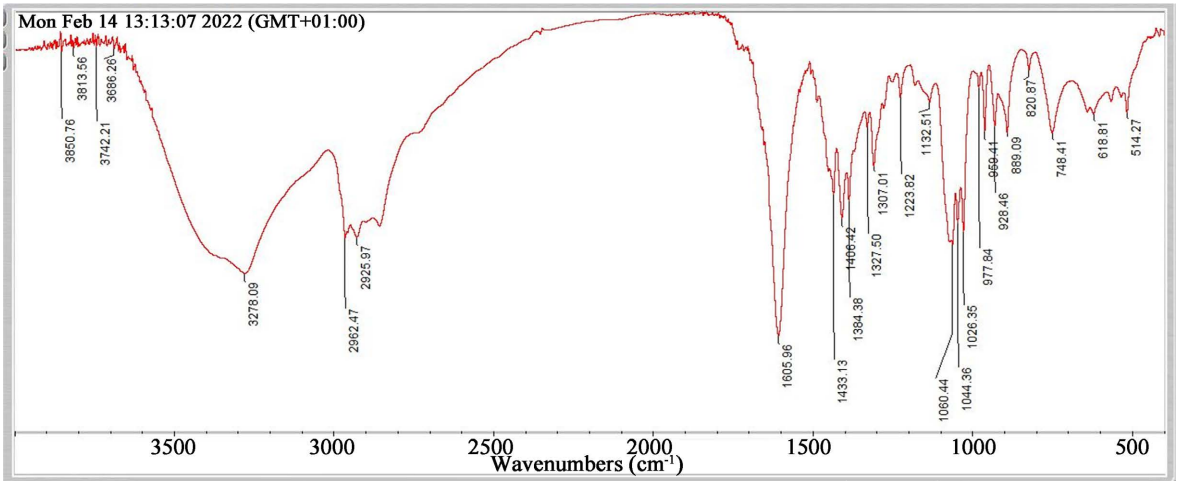

Figure 9. FTIR spectrum of Sample F [6].

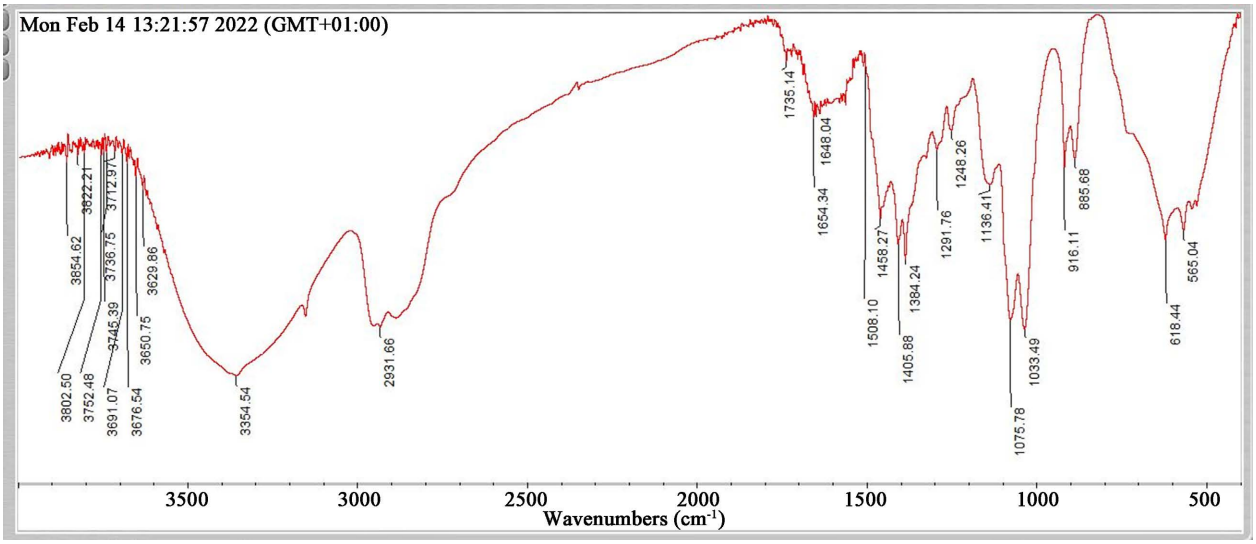

Figure 10. FTIR spectrum of Sample G [6].

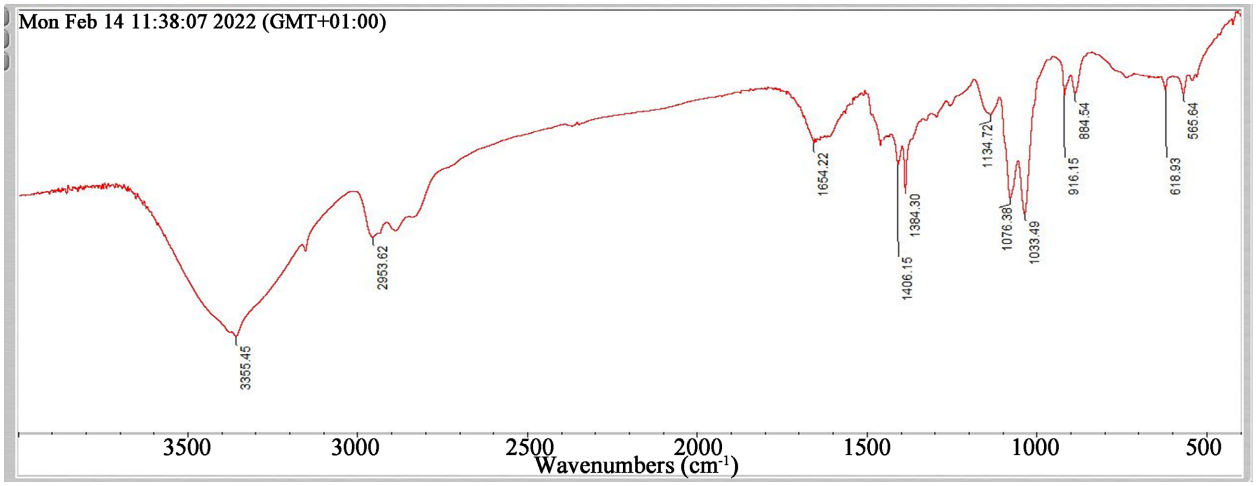

Figure 11. FTIR spectrum of Sample H [6].

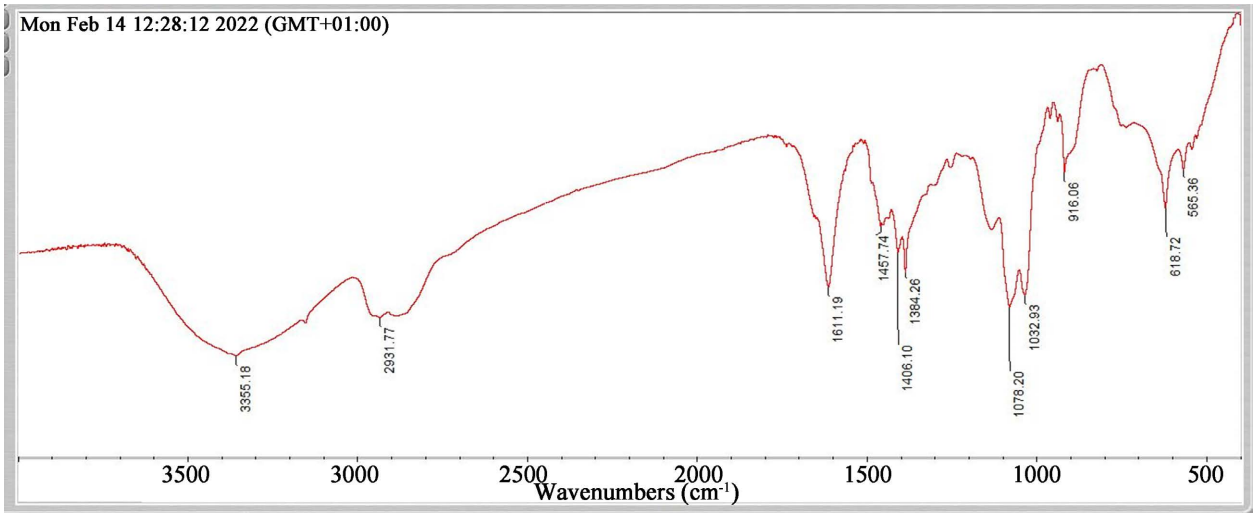

Figure 12. FTIR spectrum of Sample I [6].

absorption peaks of functional groups, display distinct characteristics. A better understanding of the growth mechanism of CZTS from metallic precursors revealed in this study provides an excellent opportunity to develop a more reliable and efficient methodology for synthesizing high-quality CZTS. In order to advance the use of wide bandgap green-synthesized copper zinc tin sulfide nanoparticles for applications in optical and electronic devices, a number of advances are needed. These include developments in synthesis and processing techniques to produce high-quality nanoparticles with desired properties, advances in characterization techniques to understand the physical and chemical properties of the particles, and advances in device fabrication to develop new devices and applications. Additionally, research into the toxicity of the nanoparticles and their environmental impact is also needed. Suggestions for future work in this project are highly recommended, and it includes: further characterization of the CZTS nanoparticles, which includes but is not limited to:

1) Scanning Electron Microscope (SEM). This SEM uses electrons instead of light to form an image that describes the sample's composition and surface topography.

2) X-ray diffraction (XRD), or x-ray powder diffraction, utilizes x-ray radiation on crystalline organic and inorganic samples. The rays are diffracted in a pattern determined by the size, arrangement, and position of the constituents of the crystalline material. This will provide us with adequate knowledge about the phase identification of the crystal and can provide information on the dimensions of the unit cell.

3) Energy-dispersive X-ray spectroscopy (EDS): this micro-analytical approach will provide us with the analysis of the element associated with electron microscopy as a result of the characteristic X-rays generated. Thus, elements in the green synthesized CZTS nanoparticles will be revealed.

The composition, surface topography, and information on the unit cell will equip us with its ability to handle higher voltages and power, higher operating temperatures, faster switching, better efficiency, and a significantly smaller form factor, which will contribute to how useful the green synthesized CZTS will be applied to optical and power devices.

Data Availability

The raw data [7] required to reproduce these findings are available to download from DOI: 10.17632/w3pp8wf9fs.1.

Conflicts of Interest

The authors declare no conflicts of interest regarding the publication of this paper.

References

[1] Yoshikawa, A., Matsunami, H. and Nanishi, Y. (2007) Development and Applica-

tions of Wide Bandgap Semiconductors. In: Takahashi, K., Yoshikawa, A. and Sandhu, A., Eds., *Wide Bandgap Semiconductors: Fundamental Properties and Modern Photonic and Electronic Devices*, Springer, Berlin, Heidelberg, 1-24. https://doi.org/10.1007/978-3-540-47235-3_1

[2] Kizilyalli, I.C., Carlson, E.P., Cunningham, D.W., Manser, J.S., Xu, Y.A. and Liu, A.Y. (2018) Wide Band-Gap Semiconductor Based Power Electronics for Energy Efficiency. US Department of Energy (USDOE), Washington DC, Advanced Research Projects Agency-Energy (ARPA-E). https://doi.org/10.2172/1464211

[3] Wide Bandgap Solutions (n.d.) Onsemi.com. https://www.onsemi.com/solutions-applications/segments/automotive/vehicle-electrification/wide-bandgap-solutions

[4] Applications of Wide Bandgap Devices (n.d.) Eepower.com. https://eepower.com/technical-articles/applications-of-wide-bandgap-devices/

[5] Makuła, P., Pacia, M. and Macyk, W. (2018) How to Correctly Determine the Band Gap Energy of Modified Semiconductor Photocatalysts Based on UV-Vis Spectra. *The Journal of Physical Chemistry Letters*, **9**, 6814-6817. https://doi.org/10.1021/acs.jpclett.8b02892

[6] Khan, S.A., Khan, S.B., Khan, L.U., Farooq, A., Akhtar, K. and Asiri, A.M. (2018) Fourier Transform Infrared Spectroscopy: Fundamentals and Application in Functional Groups and Nanomaterials Characterization. In: Sharma, S., Ed., *Handbook of Materials Characterization*, Springer, Cham, 317-344. https://doi.org/10.1007/978-3-319-92955-2_9

[7] Akanbi, O., *et al.* (2022) The Advent of Wide Bandgap Green Synthesized Copper Zinc Tin Sulfide Nanoparticles for Applications in Optical and Electronic Devices. *Mendeley Data*. https://doi.org/10.17632/w3pp8wf9fs.1